Eur. Phys. J. Plus (2017) **132**: 57
DOI 10.1140/epjp/i2017-11342-y

THE EUROPEAN PHYSICAL JOURNAL PLUS

Regular Article

Heat and mass transfer enhancement of nanofluids flow in the presence of metallic/metallic-oxides spherical nanoparticles

M. Zubair Akbar Qureshi[1,2,a], Kashif Ali[3], M. Farooq Iqbal[1], Muhammad Ashraf[1], and Shazad Ahmad[1]

[1] Centre for Advanced Studies in Pure and Applied Mathematics (CASPAM), Bahauddin Zakariya University (BZU), Multan, 608000 Pakistan
[2] Department of Computer Science, Air University, Multan Campus, Islamabad, 44000, Pakistan
[3] Department of Basic Sciences and Humanities, Muhammad Nawaz Sharif University of Engineering and Technology, Multan, Pakistan

Received: 13 November 2016 / Revised: 31 December 2016
Published online: 31 January 2017 –

Abstract. The numerical study of heat and mass transfer for an incompressible magnetohydrodynamics (MHD) nanofluid flow containing spherical shaped nanoparticles through a channel with moving porous walls is presented. Further, another endeavour is to study the effect of two types of fluids, namely the metallic nanofluid (Au + water) and metallic-oxides nanofluid (TiO_2 + water) are studied. The phenomena of spherical metallic and metallic-oxides nanoparticles have been also mathematically modelled by using the Hamilton-Crosser model. The influence of the governing parameters on the flow, heat and mass transfer aspects of the problem is discussed. The outcome of the investigation may be beneficial to the application of biotechnology and industrial purposes. Numerical solutions for the velocity, heat and mass transfer rate at the boundary are obtained and analysed.

1 Introduction

Nanofluid is a new dynamic sub-class of nanotechnology based on a heat transfer fluid, that is why the majority of the scientists and researchers are persistently attempting to take a shot at novel elements of nanotechnology. Choi [1] of Argonne National Laboratory named the amalgamation of these particulate matters of particle size in the order of nanometer "nanofluid". Nano particulate suspension in a base fluid makes it superior and finer in terms of heat transfer compared to conventional fluids. The abrasion related properties of a nanofluid are found to be excellent over the traditional fluid-solid mixture [2]. Applications of nanofluids are in vogue such as in chemical reactors, catalytic system, cooling of metallic plates, drug delivery systems, cosmetic product, paints, construction materials, cooling devices, and food. Different sorts of nanomaterials including nanowires, nanofibers and nanostructure are also utilized as a part of biotechnological applications [3].

Heat and mass transfer analysis with chemical reaction has gotten a lot of consideration lately. In the processes such as drying, separation of chemicals in distillation, evaporation, and transformation of energy in cooling tower, heat and mass transfer transpire concurrently. A chemical reaction is an imperative mechanism in material and hydrometeorological processing operations especially in the presence of nanoparticles. For example, in our atmosphere, the discharge of NO_2 from automobiles reacts chemically with unburned hydrocarbons and produces layers of photo-chemical smog (first-order homogenous chemical reaction). The chemical reaction of metallic nanoparticles with solvent and the decomposition of metallic nanoparticles is a natural phenomenon. But this decomposition affects the viscosity and fluid flow behavior of a nanofluid [4]. Das *et al.* [5] deliberated the mass transfer effect on a vertical plate in the presence of a chemical reaction. Andersson *et al.* [6] also considered the chemical reaction effect for a sheet. Heat and mass transfer analysis with the impact of a chemical reaction flow along with a semi-infinite horizontal plate on a laminar flow was discussed by Anjalidevi *et al.* [7]. Sulochana *et al.* [8] discussed the consequences of the chemical reaction on the MHD thermosolute nanofluid flow over a plate. Shehzad *et al.* [9] considered the mass transfer exploration of a non-Newtonian fluid under the inspiration of chemical reaction. The MHD chemically reacted

[a] *Present address*: Centre for Advanced Studies in Pure and Applied Mathematics (CASPAM), Bahuddin Zakariya University (BZU), Multan, Pakistan; e-mail: mzaqhashmi@gmail.com (corresponding author).

Table 1. Water and metallic/metallic-oxides nanoparticles with thermophysical properties.

	ρ (Kgm^{-3})	C_p (Jkg^{-1}K^{-1})	K (Wm^{-1}K^{-1})
H_2O	997.1	4179	0.613
Au (metallic)	19,300	1290	318
TiO_2 (metallic-oxides)	4250	686.2	8.9538

nanofluid flow for a stretching sheet was discussed by Kameswaran *et al.* [10]. With the effects of chemical reaction, the scrutiny of heat and mass transfer on a porous shrinking sheet was analysed by Muhaimin *et al.* [11]. The fortune of the injection/suction factor with relaxing/contracting porous walls of the channel in well-established flows remains a noteworthy subject in fluid mechanics that has attracted significant applications in medical and engineering sciences [12–30].

Metallic and metallic-oxides nanoparticles have immense applications in the ambit of nanosciences. Nanofluids with metallic nanoparticles have a lot of useful applications especially in medical and biological sciences. The photo-thermal metallic nanoblade is another new methodology for conveying difficult consignment into mammalian's cells. In cryosurgery undesired tissues are destroyed by penetrating the metallic nanoparticles into the target tissues. Metallic gold nanoparticles have different and distinctive shapes in which spherical, cylindrical, octahedral, nanotriangles, and nanorods are remarkable. Gold nanoparticles are finest and efficient drug-carrying molecules. Metallic-oxides have many technological applications such as the fabrication of microelectronics, circuits, sensors and fuel cells, because of their exclusive chemical and physical properties [31,32].

The principal point of this paper is to talk about the enhancement of heat and mass transfer laminar MHD incompressible nanofluid flow through a channel with porous walls with chemical reaction. Furthermore velocity, temperature and mass transfer profiles for the permeability Reynolds number as well as for a relaxing/contracting parameter with a fixed value (percentage) of the nanoparticles volume fraction are investigated. A similarity transformation technique is used to convert the governing equations into highly nonlinear ordinary differential equations, which are numerically solved by the "Shooting" method. The influence of the governing parameters on the flow, heat and mass transfer aspects of the problem is studied through graphs, whereas the thermal performance of the metallic and metallic-oxide nanofluids has been compared through tables.

2 Mathematical formulations

The thermal conductivity is the most vital thermophysical property that influences the nanofluid heat transfer rate. The thermal conductivity enhancement of nanofluids can be attributed to several factors such as volume fractions, temperature, material type, size and shape factor. The famous Maxwell model was the earliest model that was used to determine the thermal conductivity of micro/mini-particles suspended at low volume concentrations of suspensions. Nevertheless, the Maxwell model is frequently used for comparison purpose with experimental findings to its simplicity to determine the thermal conductivity of nanofluids. The Maxwell model does not take the shape of particles into consideration. An extended version of the Maxwell model was proposed by Hamilton-Crosser that includes a variable "n" known as shape factor. For example, $n = 3$ represents spherical particles, $n = 4.9$ represents needles, and $n = 6$ represents rods. Different shaped nanoparticles have significant applications and features in bio-medical sciences. The Hamilton-Crosser (H-C) model is the most common model for the effective thermal conductivity of nanofluids and is given by [33]

$$k_{nf} = k_f \left[\frac{(k_s + (n-1)k_f) - (n-1)\phi(k_f - k_s)}{(k_s + (n-1)k_f) + \phi(k_f - k_s)} \right]. \tag{1}$$

For spherical nanoparticles $\psi = 1$ or $n = 3$ and for cylindrical nanoparticles $\psi = 0.5$ or $n = 6$. Numerous theoretical works are discussed in the literature to envisage appropriate models for the effective viscosity and thermal conductivity of nanofluids [34–39].

For this problem, we consider the laminar incompressible nanofluid flow through a permeable channel of width $2a(t)$ with viscous dissipation and chemical reaction effects. The induced magnetic field is thought to be insignificant as compared to the forced field. The water is taken as a base fluid. The thermal equilibrium exists between base fluid and nanoparticles. The thermophysical properties are given in table 1. Both the channel walls are assumed to have the same permeability, and are capable of moving up or down with the time-dependent rate $a'(t)$. Therefore, the effective thermal conductivity of nanofluids is expected to enhance the heat transfer performance compared with the convectional heat transfer liquid.

The geometry of the current issue (indicated in fig. 1) shows the rectangular coordinates framework taking the origin at the centre of the channel with permeable walls which enable the fluid to enter or exit during successive

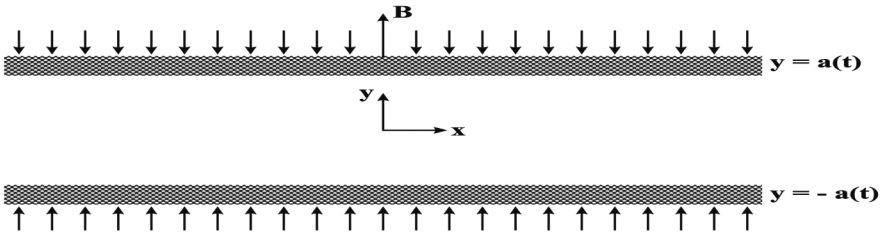

Fig. 1. Physical model of the permeable channel.

relaxation or contraction. Further, we have taken the y-axis to be perpendicular to the channel walls. Under these suppositions, the Navier-Stokes equations are

$$\frac{\partial u}{\partial x}+\frac{\partial v}{\partial y}=0, \tag{2}$$

$$\rho_{nf}\left(\frac{\partial u}{\partial t}+u\frac{\partial u}{\partial x}+v\frac{\partial u}{\partial y}\right)+\frac{\partial p}{\partial x}-\mu_{nf}\nabla^2 u+\sigma B^2 u=0, \tag{3}$$

$$\rho_{nf}\left(\frac{\partial v}{\partial t}+u\frac{\partial v}{\partial x}+v\frac{\partial v}{\partial y}\right)+\frac{\partial p}{\partial y}-\mu_{nf}\nabla^2 v=0, \tag{4}$$

$$\frac{\partial T}{\partial t}+u\frac{\partial T}{\partial x}+v\frac{\partial T}{\partial y}-\alpha_{nf}\nabla^2 T-\frac{\mu_{nf}}{(\rho C_p)_{nf}}\left(\frac{\partial u}{\partial y}\right)^2=0, \tag{5}$$

$$\frac{\partial C}{\partial t}+u\frac{\partial C}{\partial x}+v\frac{\partial C}{\partial y}-D\nabla^2 C+K_0(C-C_2)=0, \tag{6}$$

The famous Brinkman model reads as follows:

$$\upsilon_{nf}=\frac{\mu_{nf}}{\rho_{nf}}, \qquad \mu_{nf}=\frac{\mu_f}{(1-\phi)^{2.5}}, \qquad \rho_{nf}=(1-\phi)\rho_f+\phi\rho_s, \qquad \alpha_{nf}=\frac{k_{nf}}{(\rho c_p)_{nf}}, \quad \text{and}$$
$$(\rho c_p)_{nf}=(1-\phi)(\rho c_p)_f+\phi(\rho c_p)_s. \tag{7}$$

The boundary conditions are

$$\begin{aligned} &u=0;\, v=-Aa'(t), \quad \text{at} \quad y=-a(t) \quad \text{when} \quad T=T_1 \quad \text{and} \quad C=C_1,\\ &u=0;\, v=Aa'(t), \quad \text{at} \quad y=a(t) \quad \text{when} \quad T=T_1 \quad \text{and} \quad C=C_1. \end{aligned} \tag{8}$$

Here A is the wall penetrability component and the prime signifies the derivative with respect to the time.

We have used the following similarity transformation:

$$\eta=\frac{y}{a}, \qquad u=-\frac{x\nu_f}{a^2}F_\eta(\eta,t), \qquad v=\frac{\nu_f}{a}F(\eta,t), \qquad \theta=\frac{T-T_2}{T_1-T_2}, \qquad \chi(\eta)=\frac{C-C_2}{C_1-C_2}, \tag{9}$$

to reduce eqs. (3)–(6), then we introduce the following system of nonlinear ordinary differential equations:

$$\frac{\upsilon_{nf}}{\upsilon_f}F_{\eta\eta\eta\eta}+\alpha(3F_{\eta\eta}+\eta F_{\eta\eta\eta})-FF_{\eta\eta\eta}+F_\eta F_{\eta\eta}-\frac{\rho_f}{\rho_{nf}}MF_{\eta\eta}-\frac{a^2}{\upsilon_f}F_{\eta\eta t}=0, \tag{10}$$

$$\alpha_{nf}/\upsilon_f\theta_{\eta\eta}-a^2\theta_t+\theta_\eta\eta\alpha-F\theta_\eta+\left(\frac{\mu}{\rho C_p}\right)_{nf}\left(\frac{\nu^2x^2}{a^6}F^2{}_{\eta\eta}\right)=0, \tag{11}$$

$$D/\nu_f\chi_{\eta\eta}-a^2\chi_t+\chi_\eta\eta\alpha-F\chi_\eta-K_0\chi\frac{a^2}{\nu_f}=0, \tag{12}$$

whereas the boundary conditions are

$$\begin{aligned} &\eta=-1:\ F=-\,\mathrm{Re}; \quad F_\eta=0, \quad \theta=1 \quad \text{and} \quad \chi=1,\\ &\eta=-1:\ F=\mathrm{Re}; \quad F_\eta=0, \quad \theta=0 \quad \text{and} \quad \chi=0. \end{aligned} \tag{13}$$

Here T_1 and T_2 stand for the temperatures, C_1 and C_2 stand for the concentrations of the lower and upper walls of the permeable channel, respectively, with $T_1>T_2$ and $C_1>C_2$.

It is valuable to note that the proposed velocity is compatible with the continuity eq. (2). By following Majdalani *et al.* [12], we have considered the case when α is a constant, and $\theta_t = F_{\eta\eta t} = \chi_t = 0$ so that $F = F(\eta)$ and $\theta = \theta(\eta)$.

Thus, we have the following equations:

$$\frac{\upsilon_{nf}}{\upsilon_f} F_{\eta\eta\eta\eta} + \alpha(3F_{\eta\eta} + \eta F_{\eta\eta\eta}) - FF_{\eta\eta} + F_\eta F_{\eta\eta} - \frac{\rho_f}{\rho_{nf}} MF_{\eta\eta} = 0, \tag{14}$$

$$\alpha_{nf}/v_f\theta_{\eta\eta} + \theta_\eta(\eta\alpha - F) + \left(\frac{\mu}{\rho C_p}\right)_{nf} \left(\frac{\nu^2 x^2}{a^6} F^2{}_{\eta\eta}\right) = 0, \tag{15}$$

$$D/\nu_f\chi_{\eta\eta} + \chi_\eta(\eta\alpha - F) - K_0\chi\frac{a^2}{\nu_f} = 0, \tag{16}$$

Finally, adjusting $f = F/\operatorname{Re}$, we have

$$\frac{\upsilon_{nf}}{\upsilon_f} f_{\eta\eta\eta\eta} + \alpha(3f_{\eta\eta} + \eta f_{\eta\eta\eta}) - \operatorname{Re}(ff_{\eta\eta\eta} - f_\eta f_{\eta\eta}) - \frac{\rho_f}{\rho_{nf}} Mf_{\eta\eta} = 0, \tag{17}$$

$$\frac{K_{nf}}{K_f}\theta_{\eta\eta} + \left(\frac{(\rho C_p)_{nf}}{(\rho C_p)_f}\right) pr\cdot\theta_\eta(\eta\alpha - \operatorname{Re} f) + (1-\phi)^{-2.5}\operatorname{Pr} Ec\operatorname{Re}^2 {f_{\eta\eta}}^2 = 0, \tag{18}$$

$$\chi_{\eta\eta} + Sc\cdot\chi_\eta(\eta\alpha - \operatorname{Re} f) - K_r\chi(\eta) = 0, \tag{19}$$

which are then converted to the nanoparticles volume fraction form

$$[Z_1(\phi)Z_2(\phi)](f_{\eta\eta\eta\eta} - f_{\eta\eta}) + \alpha(3f_{\eta\eta} + \eta f_{\eta\eta\eta}) - \operatorname{Re}(ff_{\eta\eta\eta} - f_\eta f_{\eta\eta}) - Z_2(\phi)\cdot Mf_{\eta\eta} = 0, \tag{20}$$

$$K(\phi)\theta_{\eta\eta} + Z_3(\phi)(\eta\alpha - \operatorname{Re} f)\operatorname{Pr}\theta_\eta + Z_1(\phi)\cdot Ec\cdot\operatorname{Re}^2\cdot\operatorname{Pr}\cdot{f_{\eta\eta}}^2 = 0, \tag{21}$$

$$\chi_{\eta\eta} + Sc\chi_\eta(\eta\alpha - \operatorname{Re} f) - \chi(\eta)\cdot K_r = 0, \tag{22}$$

with the boundary conditions

$$\begin{aligned} &\eta = -1: \ f = -1; \quad f_\eta = 0, \quad \theta = 1 \quad \text{and} \quad \chi = 1, \\ &\eta = -1: \ f = 1; \quad f_\eta = 0, \quad \theta = 0 \quad \text{and} \quad \chi = 0. \end{aligned} \tag{23}$$

Here $\alpha = \frac{a(t)a'(t)}{\upsilon}$ is the dimensionless time-dependent relaxation/contraction parameter, and is positive in case of contraction whereas it acquires a negative value if relaxation exists. In our problem, we take $Aa'(t) = \upsilon_w$, then the permeable Reynolds number becomes $\operatorname{Re} = a(t)\upsilon_w/\upsilon_f < 0$ for the suction case and $\operatorname{Re} = a(t)\upsilon_w/\upsilon_f > 0$ for the injection case as well [12], where

$$Z_1(\phi) = (1-\phi)^{-2.5}, \quad Z_2(\phi) = \left(1 - \phi + \phi\frac{\rho_s}{\rho_f}\right)^{(-1)} \quad \text{and} \quad Z_3(\phi) = \left(1 - \phi + \phi\frac{(\rho C_p)_s}{(\rho C_p)_f}\right).$$

3 Numerical procedure

A numerical technique, 4th-order Runge-Kutta method along with the shooting methodology, has been applied to solve the system of nonlinear coupled equations (20)–(22) with boundary conditions (23). Before applying the numerical method, we convert the governing ODEs into a system of first-order ODEs, as follows:

We put $f' = a$, $f'' = b$, $f''' = c$, $\theta' = d$, $\chi' = e$, in eqs. (20)–(22), we have $f' = a$, $a' = b$, $b' = c$.

$$\begin{aligned} c' &= b + (Z_1(\phi)Z_2(\phi))^{-1}[Z_2(\phi)Mb + \operatorname{Re}(fc - ab) - \alpha(3b + \eta c)], \\ d' &= -Z_3(\phi)K(\phi)^{-1}[(\eta\alpha - \operatorname{Re} f) + Z_1(\phi)Ec\cdot\operatorname{Re}^2\cdot\operatorname{Pr}\cdot b^2]\operatorname{Pr}, \\ e' &= K_r\chi(\eta) - Sc(\eta\alpha - \operatorname{Re} f)e. \end{aligned} \tag{24}$$

With the following obligatory boundary conditions:

$$f(-1) = -1,\ a(-1) = -1,\ \theta(-1) = 1,\ \chi(-1) = 1,\ b(-1) = \Theta 1,\ c(-1) = \Theta 2,\ d(-1) = \Theta 3,\ e(-1) = \Theta 4. \tag{25}$$

Here $\Theta 1$, $\Theta 2$, $\Theta 3$ and $\Theta 4$ are missing initial conditions. Therefore, at this stage, a shooting method is very effective to find out the unknown initial conditions with the least computational cost.

Table 2. Effects of Re when $\alpha = -1$, $\phi = 0.06$, $C = 0.1$, $Ec = 0$, $M = 1$, $Sc = 1$ and Pr = 6.2.

	Metallic (Au) nanofluid			Metallic-oxides (TiO_2) nanofluid		
Re	$f''(-1)$	$\theta'(-1)$	$\chi'(-1)$	$f''(-1)$	$\theta'(-1)$	$\chi'(-1)$
-1	4.19168	-0.36988	-0.534916	3.79044	-0.670328	-0.533192
-0.5	4.40338	-0.968884	-0.646375	3.88796	-0.232989	-0.645197
0	4.64876	-1.98464	-0.774948	3.99511	-0.067143	-0.774948
0.5	4.93215	-3.26874	-0.921499	4.11279	-0.017251	-0.923564
1	5.25781	-4.63023	-1.086630	4.24191	-0.004179	-1.091930

Table 3. Effects of Re when $\alpha = 1$, $\phi = 0.06$, $K_r = 0.1$, $Ec = 0$, $M = 1$, $Sc = 1$ and Pr = 6.2.

	Metallic (Au) nanofluid			Metallic-oxides (TiO_2) nanofluid		
Re	$f''(-1)$	$\theta'(-1)$	$\chi'(-1)$	$f''(-1)$	$\theta'(-1)$	$\chi'(-1)$
-1	2.00603	-0.0041705	-0.263183	2.4028	-4.88222	-0.264688
-0.5	1.93151	-0.018048	-0.327239	2.39578	-3.44875	-0.328265
0	1.83493	-0.072609	-0.405111	2.38764	-2.06276	-0.405110
0.5	1.70716	-0.25609	-0.498917	2.37817	-0.954408	-0.497002
1	1.53430	-0.730132	-0.610916	2.36712	-0.329077	-0.605664

4 Results and discussion

The numerical shooting technique has been duly applied on nonlinear coupled equations (24) by using NDSolve in Mathematica. The shear stress, heat and mass transfer rates at the lower wall of the permeable channel are the physical quantities which are directly proportional to $f''(-1)$, $\chi'(-1)$ and $\theta'(-1)$, respectively. The dynamic parameters required for the current study are the permeable Reynolds number Re, the magnetic parameter M, the Eckert number Ec, expansion/contraction ratio α, the Schmidt number Sc, the nanoparticles volume fraction parameter ϕ, and the chemical reaction parameter K_r. Further, the values of different parameters have been taken arbitrarily, as done in the literature. In one of our recent studies (Akbar *et al.* [40]), we have noted that the thermal performance of the spherical shaped particles was found to be better than that of the cylindrical shaped particles. That is why we have used the spherical shaped particles in the present study. Further, the most commonly used ranges for the different non-dimensional parameters are $0 \leq \phi \leq 0.1$, Re $= \{-1, -0.5, 0.5, 1\}$, $M = \{2, 4, 6, 8\}$, $Ec = \{0.1, 0.2, 0.3, 0.4\}$, $\alpha = \{-2, -1, 1, 2\}$, $Sc = \{0.5, 1, 1.5, 2\}$ and $K_r = \{0.2, 0.4, 0.6, 0.8\}$.

The study will focus the impact of the physical parameters on the quantities $f''(-1)$, $\theta'(-1)$ and $\chi'(-1)$ through tables 2–5. The graphs have been designed to determine the effect of the said parameters on the velocity, temperature and concentration profiles $f'(\eta)$, $\theta(\eta)$ and $\chi(\eta)$, respectively.

Tables 2 and 3 show the effect of the Reynolds number Re on the physical quantities at the lower wall of the porous channel under the influence of chemical reactions. When $\alpha < 0$, for a metallic nanofluid (Au-water), it is observed an increasing behaviour of shear stress for the injection case, whereas an opposite trend exists for heat and mass transfer rates, and a decreasing pattern of shear stress is detected for the suction case while the trend observed for heat and mass transfer rates is quite opposite. Now for the metallic-oxides nanofluid (TiO_2-water) case, mass transfer rate increases and shear stress and heat transfer rate decrease when suction exits, an opposite trend is observed for the injection case. In the case of $\alpha > 0$, it is clear from table 3 for the metallic (Au-water) nanofluid that shear stress, heat and mass transfer rates increase for the suction case but an opposite behavior is observed for the injection case. Now for the metallic-oxides (TiO_2-water) nanofluid, shear stress and mass transfer rates increase for the suction case and decrease for the injection case as well. But the most important aspect is that the heat transfer rate showed a quite opposite behavior for injection and suction cases.

Tables 4 and 5 show the influence of the chemical reaction on the mass transfer rate for metallic and metallic-oxides nanofluids with injection and suction factor, respectively. The chemical reaction and mass transfer rate are very much interlinked. As K_r increases, the mass transfer rate decreases for the metallic (Au-water) nanofluid, whereas an opposite trend is noted for the metallic-oxides (TiO_2-water) nanofluid. Figure 2 clearly describes the comparison

Table 4. Effects of the chemical reaction on the mass transfer for the metallic nanofluid.

	$\chi'(-1)$ for Au			
	Re = 1		Re = −1	
K_r	$\alpha = -1$	$\alpha = 1$	$\alpha = -1$	$\alpha = 1$
0.2	−1.19492	−0.675939	−0.594567	−0.301009
0.4	−1.38521	−0.796358	−0.70633	−0.373952
0.6	−1.5485	−0.906037	−0.800496	−0.44363
0.8	−1.69157	−1.00693	−0.905457	−0.510402
1.0	−1.81894	−1.10052	−0.995303	−0.574572

Table 5. Effects of the chemical reaction on the mass transfer for the metallic-oxides nanofluid.

	$\chi'(-1)$ for TiO_2			
	Re = 1		Re = −1	
K_r	$\alpha = -1$	$\alpha = 1$	$\alpha = -1$	$\alpha = 1$
0.2	−1.20075	−0.70333	−0.592737	−0.302584
0.4	−1.39175	−0.7902138	−0.704332	−0.375645
0.6	−1.55547	−0.899523	−0.807376	−0.445418
0.8	−1.69875	−1.00017	−0.903279	−0.512266
1.0	−1.82627	−1.09359	−0.993033	−0.576995

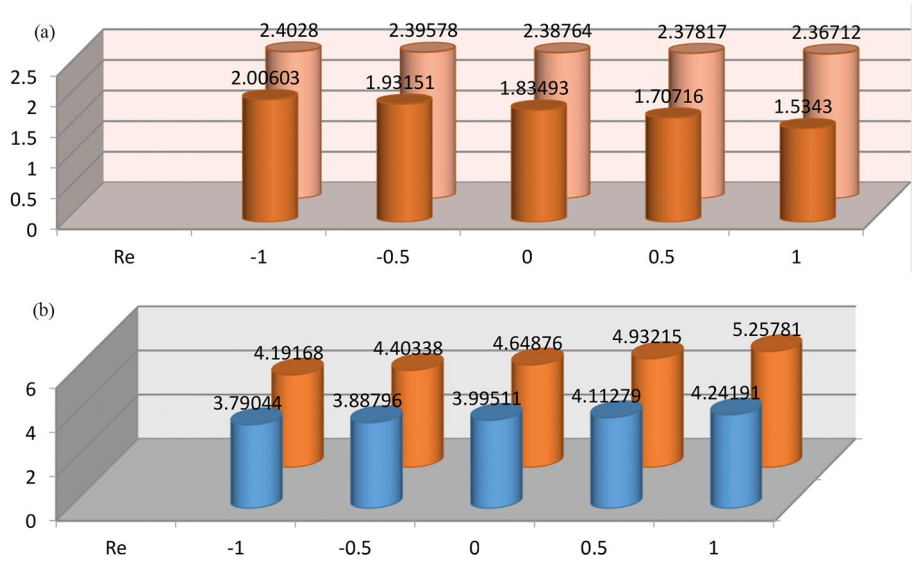

Fig. 2. (a) Effects of Re on shear stress for metallic and metallic-oxides when $\alpha < 0$. Light brown/brown for metallic/metallic-oxides. (b) Effects of Re on shear stress for Metallic/Metallic-oxides when $\alpha > 0$. Red/blue for metallic/metallic-oxides.

of the shear stress at the lower wall of the channel for the metallic as well as the metallic-oxides nanofluid with the effect of permeable Reynolds numbers. Note that the shear stress in the case of the metallic nanofluid is higher than that of the non-metallic nanofluid. As the injection increases the difference between the shear stress of metallic and the metallic-oxides becomes larger for the relaxation case. A similar behavior is observed for the contraction case. The difference between the shear stresses of the metallic (Au-water) nanofluid for the contraction case is significant as compared to the relaxation of the porous walls.

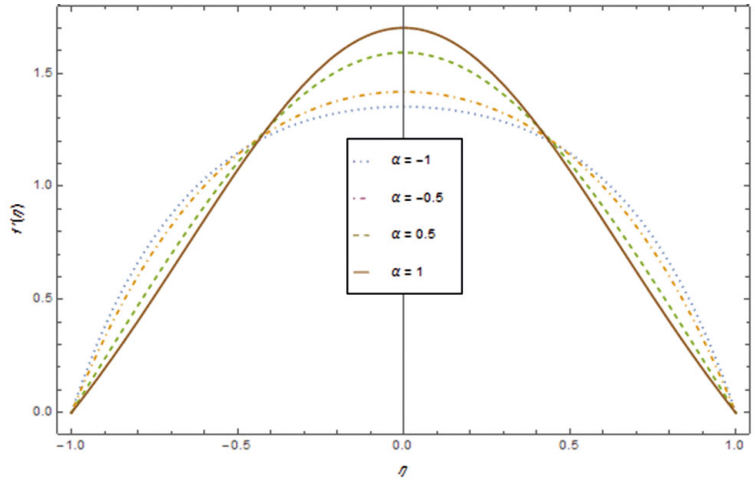

Fig. 3. Velocity profile for Re $= -1$, $Ec = 0.01$, $\phi = 0.1$, $K_r = 0.1$, $M = 1$.

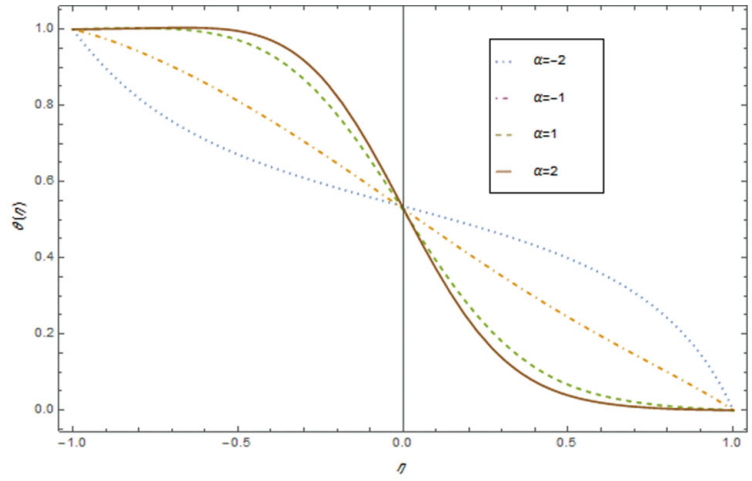

Fig. 4. Temperature profile for Re $= -1$, $Ec = 0.01$, $\phi = 0.1$, $K_r = 0.1$, $M = 1$.

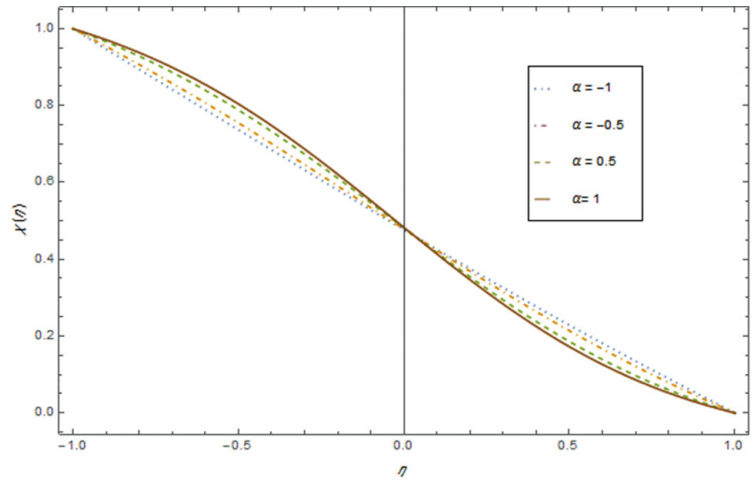

Fig. 5. Mass transfer profile for Re $= -1$, $Ec = 0.01$, $\phi = 0.1$, $K_r = 0.1$, $M = 1$.

Figures 3–5 show the effect of α on velocity, heat and mass transfer profiles in the presence of nanoparticles and chemical reaction, respectively. Figure 3 depicts that the $f'(\eta)$ velocity profile increases with the increase of α when $-0.5 < \eta < 0.5$, while it decreases for $\eta > 0.5$ or < -0.5. Thermal and concentration boundary layer thickness increase as the values of α increase as shown in figs. 4 and 5 respectively. Figures 6–9 are plotted to explore the variation in temperature for different values of ϕ, Re, Pr and Ec with the chemical reaction effects. It can be clearly seen in fig. 6

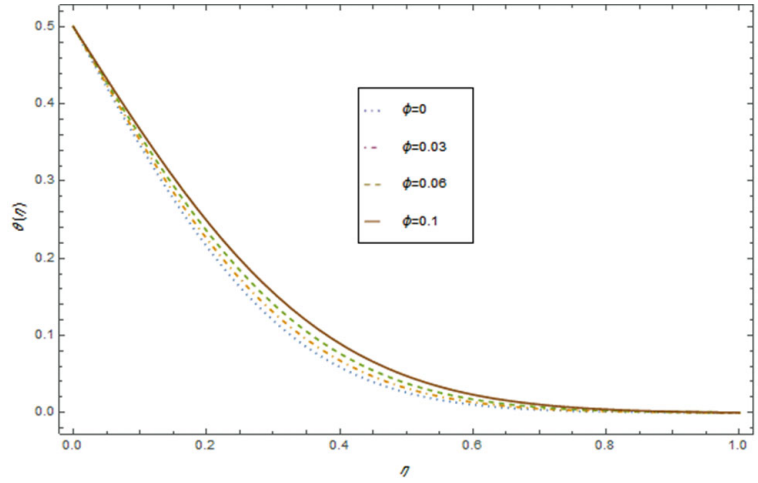

Fig. 6. Temperature profile for $\mathrm{Re} = -1$, $Ec = 0.01$, $\alpha = 1$, $K_r = 0.1$, $M = 1$.

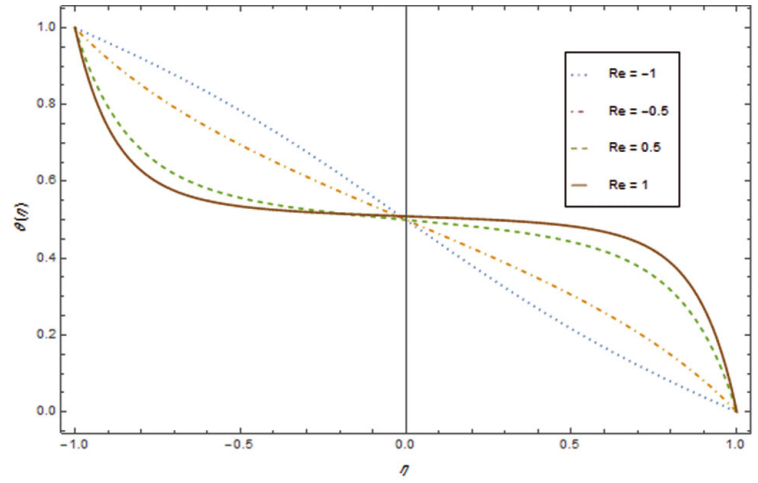

Fig. 7. Temperature profile for $\phi = 0.1$, $Ec = 0.01$, $\alpha = 1$, $K_r = 0.1$, $M = 1$.

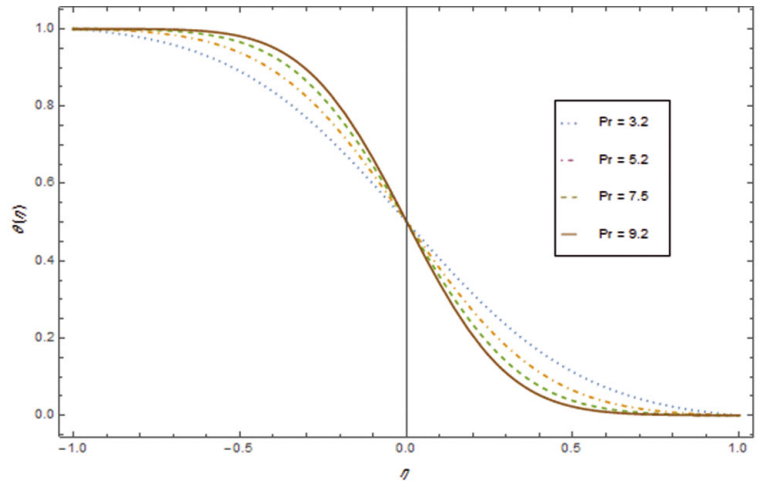

Fig. 8. Temperature profile for $\phi = 0.1$, $Ec = 0.01$, $\alpha = 1$, $K_r = 0.1$, $M = 1$, $\mathrm{Re} = -1$.

that with the increase in ϕ, a visible increase can be seen in the thermal boundary layer thickness, whether porous walls are moving away or converging to each other. As can be understood from fig. 7, as Re increases, the thermal boundary layer thickness also decreases. The maximum temperature profile is found to increase when the permeable Reynolds number is enhanced. Figure 8 shows that the temperature profile is an increasing function of the Prandtl number. Actually Pr is the ratio of momentum and thermal diffusivity. Thermal diffusivity enhances for the small

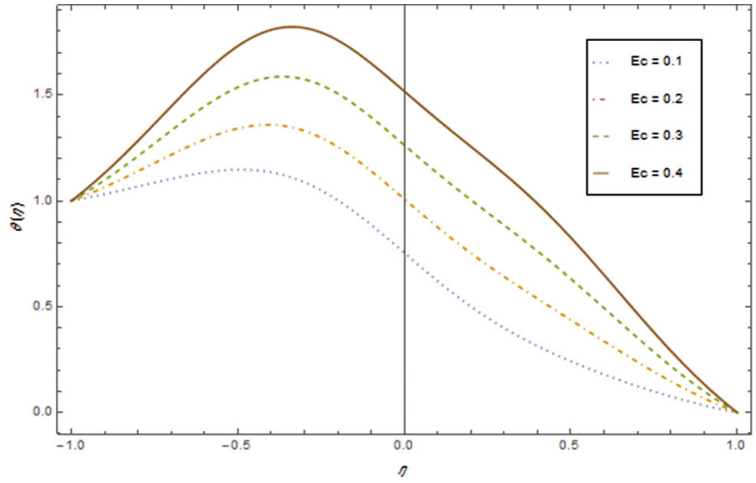

Fig. 9. Temperature profile for $\phi = 0.1$, $\alpha = 1$, $K_r = 0.1$, $M = 1$, $\mathrm{Re} = -1$, $Sc = 1$.

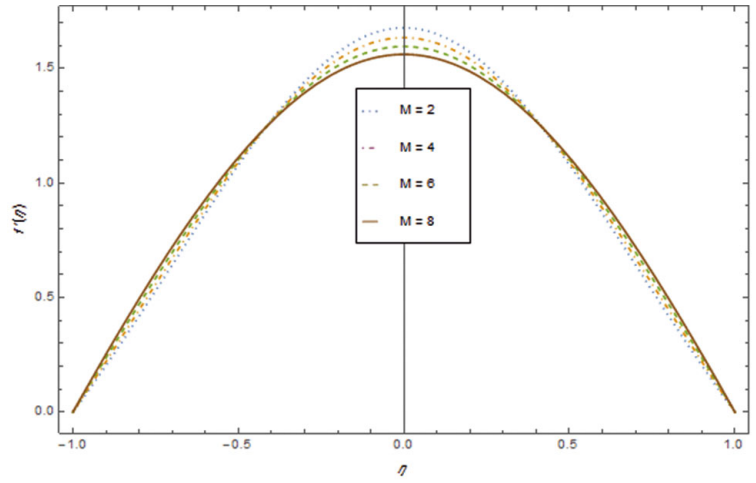

Fig. 10. Velocity profile for $\phi = 0.1$, $\alpha = 1$, $\mathrm{Re} = -1$, $Sc = 1$.

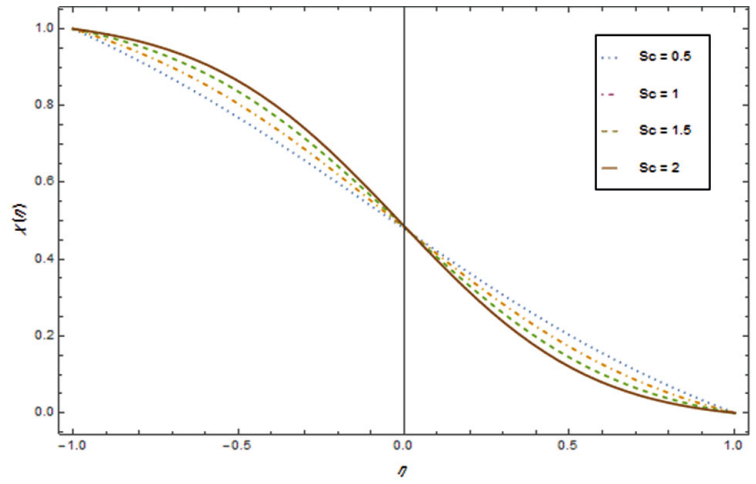

Fig. 11. Mass transfer profile for $\phi = 0.1$, $\alpha = 1$, $K_r = 0.1$, $M = 1$, $\mathrm{Re} = -1$.

values of Pr while momentum diffusivity is increased. Figure 9 shows the remarkable effect of the Eckert number on the temperature profile. The Ec describes the association between a flow of kinetic and enthalpy. As Ec increases, the temperature profile also increases significantly in the permeable channel, no issue the walls are approaching or retreating. The Eckert number and temperature profile are very much interdependent. Increasing values of M result in a considerable lowering of the velocity profile due to the Lorentz force (drag force) in the middle of the permeable

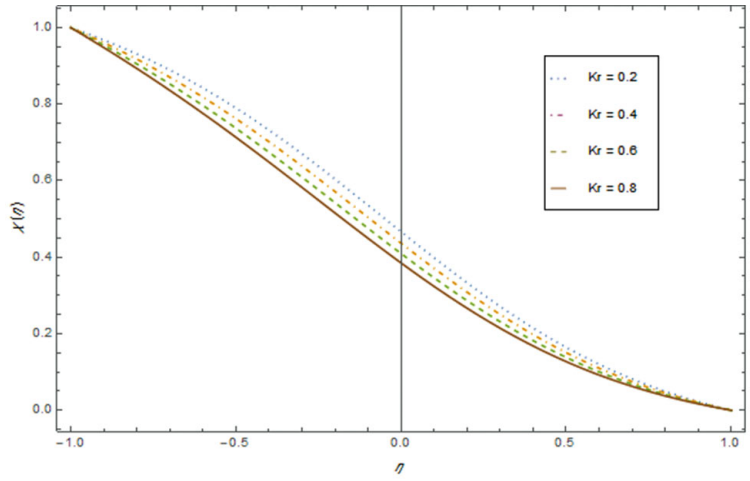

Fig. 12. Mass transfer profile for $\phi = 0.1$, $\alpha = 1$, $M = 1$, $\mathrm{Re} = -1$, $Sc = 1$.

channel between the two porous walls as shown in fig. 10. As Sc increases, the concentration boundary layer thickness is also affected in the form of its increase as shown in fig. 11. Increasing phenomena exist between mass transfer profile and chemical reaction. Figure 12 shows a significant increase in the mass transfer profile when the chemical reaction parameter is increased.

5 Conclusions

The problem of a viscous dissipative MHD nanofluid flow through a permeable channel is examined numerically for two types of nanoparticles (gold and titanium oxide). The influence of the governing parameters (namely, the Reynolds number, the magnetic parameter, the Eckert number, the wall expansion/contraction ratio, the Schmidt number, the nanoparticles volume fraction parameter, and the chemical reaction parameter) on the momentum as well as on the heat and mass transfer characteristics of the problem has been discussed. The following conclusions may be drawn from the study:

- In case of approaching walls, the shear stress as well as the heat and mass transfer rates (for the gold nanofluid) at the channel walls increase with injection, whereas an opposite effect is noticed for suction.
- For the nanofluid with titanium oxide particles, the trend is the same for the shear stress and the mass transfer only.
- For both the types of nanofluid, the chemical reaction parameter always increases the mass transfer, no matter the channel walls are approaching or receding.
- The external magnetic field acts like a drag force which tends to slow down the fluid motion while raising the temperature distribution across the channel.

We are very thankful to the Higher Education Commission (HEC) of Pakistan and Air University, (Islamabad, Pakistan) for providing the research environment and sufficient resources in order to conduct this study.

Authors contribution statement

All authors have equally contributed in this work. All authors read and approved the final manuscript.

Conflict of interests

The authors declare that “they have no competing interests”.

Nomenclature

A:	permeability component		
B:	the external uniform magnetic field		
C:	mass concentration	$\mathrm{Re} = \frac{Aaa'}{2\upsilon_f}$:	the permeability Reynolds number
D:	mass diffusivity coefficient		
p:	pressure	$\mathrm{Pr} = \frac{(\mu c_p)_f}{k_f}$:	the Prandtl number
T:	fluid temperature		
F:	self-similar velocity		
k_s:	thermal conductivity of solid fractions	$\mu_{nf} = \frac{\mu_f}{(1-\phi)^{2.5}}$:	the dynamic viscosity of the nanofluid
k_f:	thermal conductivity of the fluid	$\rho_{nf} = (1-\phi)\rho_f + \phi\rho_s$:	the density of the nanofluid
k_{nf}:	thermal conductivity of the nanofluid	*Greek symbols*	
n:	depends on the shape factor through the H-C model	$\alpha = \frac{aa'(t)}{\upsilon_f}$:	the wall expansion ratio
		η:	scaled boundary layer coordinate
ρ_s:	the density of the solid fractions	θ:	self-similar temperature
c_p:	specific heat at constant pressure	χ:	self-similar mass transfer
$(c_p)_{nf}$:	specific heat for the nanofluid	ϕ:	nanoparticle volume fraction parameter
Dimensionless number		μ:	dynamic viscosity
$M = \frac{\sigma B^2 a^2}{\mu_f}$:	magnetic parameter	υ:	kinematic viscosity
$Sc = \frac{\upsilon_f}{D}$:	schmidt number	ρ:	density
$K_r = \frac{K_0 a^2}{D}$:	chemical reaction parameter	σ:	electric conductivity
$Ec = \frac{(\nu x)^2}{\Delta T a^2 (Cp)_f}$:	Eckert number	*Subscripts*	
α_{nf}:	thermal conductivity for the nanofluid	nf:	nanofluid
		f:	fluid phase
$(\rho)_{nf}$:	density for the nanofluid	s:	solid phase
$(\upsilon)_{nf}$:	kinematic viscosity for the nanofluid	w:	conduction at wall

References

1. K. Das, S.U.S. Choi, *Nanofluids: Science and Technology* (Wiley, New Jersey, 2007).
2. A.J. Chmakha *et al.*, J. Nanofluids **4**, 271 (2015).
3. M. Lomascolo *et al.*, Renew. Sustain. Energy **43**, 1182 (2015).
4. G.V.P.N. Srikantha *et al.*, Proc. Mater. Sci. **10**, 10 (2015).
5. U.N. Das *et al.*, Forsch. Ingenieurwes. **60**, 284 (1994).
6. H.I. Andersson *et al.*, Int. J. Heat Mass Transfer **37**, 659 (1994).
7. S.P. Anjalidevi *et al.*, Z. Angew. Math. Mech. **80**, 697 (2000).
8. C .Sulochana *et al.*, Chem. Proc. Eng. Res. **34**, 28 (2015).
9. S.A. Shehezad *et al.*, Braz. J. Chem. Eng. **30**, 187 (2013).
10. P.K. Kameswaran *et al.*, Int. J. Heat Mass Transfer **55**, 7587 (2012).
11. R. Muhaimin *et al.*, Nucl. Eng. Design **240**, 2699 (2010).
12. J. Majdalani *et al.*, J. Biomech. **35**, 1399 (2002).
13. M. Sheikholeslami *et al.*, Powder Technol. **246**, 327 (2013).
14. M. Fakour *et al.*, J. Mol. Liq. **204**, 198 (2015).
15. M. Hatami *et al.*, J. Mol. Liq. **187**, 294 (2013).
16. M. Hatami, D.D. Ganji, J. Mol. Liq. **190**, 159 (2013).

17. M. Sheikholeslami *et al.*, J. Magn. & Magn. Mater. **349**, 188 (2014).
18. M. Sheikholeslami *et al.*, J. Mol. Liq. **193**, 174 (2014).
19. M. Sheikholeslami *et al.*, Powder Technol. **256**, 490 (2014).
20. M. Sheikholeslami *et al.*, Int. J. Heat Mass Transfer **92**, 339 (2016).
21. M. Sheikholeslami *et al.*, Comput. Fluids **94**, 147 (2014).
22. M. Sheikholeslami *et al.*, J. Magn. & Magn. Mater. **374**, 36 (2015).
23. T. Hayat *et al.*, J. Magn. & Magn. Mater. **385**, 222 (2015).
24. T. Hayat *et al.*, AIP Adv. **5**, 067169 (2015).
25. T. Hayat *et al.*, J. Mol. Liq. **194**, 93 (2014).
26. M.M. Rashidi *et al.*, J. Mol. Liq. **198**, 234 (2014).
27. Z. Mehrez *et al.*, J. Magn. & Magn. Mater. **374**, 214 (2015).
28. F. Mabood *et al.*, J. Magn. & Magn. Mater. **374**, 569 (2015).
29. F.M. Abbasi *et al.*, AIP Adv. **5**, 037111 (2015).
30. S.A. Shehzad *et al.*, PLoS ONE **9**, 0111417 (2014).
31. M. Hatami *et al.*, Comput. Method Program Biomed. **113**, 632 (2014).
32. A.K. Khan *et al.*, Trop. J. Pharm. Res. **13**, 1169 (2014).
33. R.L. Hamilton *et al.*, Ind. Eng. Chem. Fundam. **1**, 187 (1962).
34. S.P. Jhang, S.U.S. Choi, J. Heat Transfer **129**, 617 (2006).
35. S.K. Das *et al.*, J. Heat Transfer **125**, 567 (2003).
36. G. Aaiza *et al.*, Nanoscale Res. Lett. **10**, 490 (2015).
37. C. Kleinstreuer, Y. Feng, Nanoscale Res. Lett. **6**, 229 (2011).
38. R. Hentschke, Nanoscale Res. Lett. **11**, 88 (2016).
39. K. Saisdhan, J. sang, Nanoscale Res. Lett. **6**, 239 (2011).
40. M. Zubair Akbar *et al.*, AIP Adv. **6**, 045222 (2016).